

Scrambling and entanglement spreading in long-range spin chains

Silvia Pappalardi,^{1,2,*} Angelo Russomanno,^{2,3} Bojan Žunkovič,⁴ Fernando Iemini,^{2,5} Alessandro Silva,¹ and Rosario Fazio^{2,3}

¹SISSA, Via Bonomea 265, I-34135 Trieste, Italy

²Abdus Salam ICTP, Strada Costiera 11, I-34151 Trieste, Italy

³NEST, Scuola Normale Superiore & Istituto Nanoscienze-CNR, I-56126 Pisa, Italy

⁴Faculty of Mathematics and Physics, University of Ljubljana, Jadranska 19, SI-1000 Ljubljana, Slovenia

⁵Instituto de Física, Universidade Federal Fluminense, 24210-346 Niterói, Brazil



(Received 7 June 2018; revised manuscript received 7 September 2018; published 8 October 2018)

We study scrambling in connection with multipartite entanglement dynamics in regular and chaotic long-range spin chains, characterized by a well-defined semi-classical limit. For regular dynamics, scrambling and entanglement dynamics are found to be very different: up to the Ehrenfest time, they rise side by side, departing only afterward. Entanglement saturates and becomes extensively multipartite, while scrambling, characterized by the dynamic of the square commutator of initially commuting variables, continues its growth up to the recurrence time. Remarkably, the exponential growth of the latter emerges not only in the chaotic case but also in the regular one, when the dynamics occurs at a dynamical critical point.

DOI: [10.1103/PhysRevB.98.134303](https://doi.org/10.1103/PhysRevB.98.134303)

I. INTRODUCTION

Classical systems with long-range interactions display many interesting dynamical properties that have been extensively studied for many decades [1]. In the quantum domain, instead, long-range systems have been the focus of a great deal of attention only lately, as a result of their experimental simulation with different platforms [2–5]. These systems allow the controlled study of quantum dynamics in the absence of significant decoherence, a property that allows the study of a number of important phenomena as, for example, dynamical phase transitions (DPTs) [6–8] or the dynamics of correlations [9–13] in a situation where Lieb-Robinson bounds do not apply [14,15].

It is well established that understanding the coherent dynamics of a quantum many-body system requires a thorough understanding of the behavior of its quantum correlations [16,17]. The *spreading of quantum correlations* has been the focus of a lot of theoretical efforts [18], starting from the initial important results on the dynamics of entanglement entropy [19]. Very recently, a new way to characterize quantum dynamics of many-body systems has been proposed, based on the concept of *scrambling*. Initially introduced as a probe of quantum chaos [20–23], scrambling is generically identified as the delocalization of quantum information [24] in a many-body system. A measure of scrambling is associated with the growth of the square commutator between two initially commuting observables [20,21]. For quantum chaotic systems [20,21,25,26], this quantity is expected to grow exponentially before the Ehrenfest time — defined as the time at which semiclassical breaks and quantum effects become dominant [56] — otherwise, it grows, at most, polynomially in time [27–29].

Despite the impressive progress over the last years, several different questions related to scrambling and entanglement propagation still await a more detailed answer. It has been observed that the exponential growth of the square commutator is connected to the chaotic behavior of an underlying semiclassical limit. The precise role of semiclassical correlations in determining scrambling dynamics and its various stages are presently under intense study [30–32]. Furthermore, in view of the various forms in which quantum correlations manifest in a many-body system, it is important to understand how entanglement is connected to the scrambling of information. A first connection between square commutators and the spreading of quantum entanglement has been made in the context of unitary quantum channels [33,34]. An analysis of different velocities of propagation of information has been performed in Ref. [24], while connections of scrambling to the growth of Rényi entropies and multiple-quantum coherence spectra have been investigated in Refs. [35–37]. In long-range systems, scrambling has been studied in connection with correlation bounds [13,38] and its time average as a probe of criticality [39]. However, an analysis of the dynamics and the relevant timescales in relation to the different processes involved in the spreading of information is still missing.

In this paper, we address all these questions by studying multipartite entanglement propagation and scrambling in spin chains with long-range interaction, either subject to a quantum quench or a periodic drive. There are several reasons behind this choice. Spin chains with long-range interactions possess a well-defined semiclassical limit, and thus represent a natural playground [40] to study the role of classical correlations in scrambling. Furthermore, they allow exploration of the transition from semiclassical to quantum dominated regimes in the dynamical behavior. We will consider both the case of integrable and chaotic dynamics. Moreover, scrambling is experimentally accessible with long-range quantum simulators, as it has been measured for unitary operators [41]. We will present results for the entanglement dynamics of the quantum Fisher

*spappala@sissa.it

information (QFI), the tripartite mutual information (TMI), and operator scrambling, studied via the square commutator. As we are going to show in the rest of the paper, scrambling and entanglement dynamics turn out to be very different.

The paper is organized as follows. The next section is devoted to a summary of the results with a direct comparison between multipartite entanglement growth and scrambling. In Sec. III, we review the long-range version of the Ising chain and the types of dynamics that are considered across the paper. We recall the semiclassical limit together with the quantum and classical characterization of chaos. In Sec. IV, we briefly review the definitions of the quantities under consideration: the QFI, the TMI, and the square commutator. In Sec. V, we describe the different numerical and the semianalytical methods used to reproduce the behavior of the square commutator. We first present in Sec. VIA the results for the entanglement dynamics and its semiclassical nature for sufficiently long-range interaction. We discuss how this behavior changes when the range of the interaction is decreased. Then, in Sec. VIB, we consider the results for the square commutator and we argue that the long-time dynamics of the square commutator accounts for the quantum chaoticity of the dynamics. We provide evidence for our claims by discussing an example of exponential growth of scrambling in the case of a regular quantum dynamics. Section VII is devoted to our conclusions.

II. MAIN RESULTS

In this paper, we study how entanglement and operator scrambling grow and spread in Ising spin chains with two-body power-law decaying interactions, $J_{ij} \propto |i - j|^{-\alpha}$. We consider the case in which an initial separable state, i.e., $|\psi_0\rangle = |\uparrow\uparrow\dots\uparrow\rangle$, is brought out-of-equilibrium by means of a quantum quench or a periodic drive. Our findings can be summarized as follows:

(1) Entanglement dynamics reflects the semiclassical nature of the system: it is weak, slow growing, and saturating at the Ehrenfest time t_{Ehr} . This is what lies at the heart of the classical “simulability” of quantum long-range interacting systems in the context of MPS-TDVP [42,43] with small bond-dimension as well as semiclassical methods [44–46].

(2) The square commutator is characterized by two different regimes, a first semiclassical growth up to the t_{Ehr} (exponential for chaotic dynamics), followed by a fully quantum nonperturbative polynomial growth (saturation for chaotic dynamics), symmetric around $t^* = t_{\text{rec}}/2$ the *recurrence time* t_{rec} . We show that the initial growth encodes the nature of classical orbits and can be exponential also for regular integrable dynamics, provided they have some classical instabilities. Conversely, the second regime accounts for the quantum chaoticity of the dynamics, see Table I.

(3) The dynamics of the information spreading changes with the range of interaction α . The Hamiltonian with $0 \leq \alpha < 1$ is dominated by the classical limit and the structure of entanglement and scrambling is the same as in the infinite range case, see Table I. For $1 \leq \alpha < 2$, the entanglement grows linearly in time and the structure of the asymptotic state is the same as for $\alpha < 1$. For $\alpha \geq 2$, the state displays the typical entanglement dynamics and structure of short-range interacting systems, with negative TMI.

TABLE I. Scrambling and entanglement dynamics for the different protocols with the infinite range Hamiltonian. While, for all the types of dynamics, entanglement grows and saturates at t_{Ehr} , scrambling continues its growth in the regular case. Particularly interesting is that, despite the dynamics being regular, the early-time exponential behavior emerges when the dynamics occurs at the critical point of the dynamical phase transition (DPT), see Fig. 8. The Ehrenfest time and the recurrence time depend on the dynamics too: $t_{\text{Ehr}} \propto \sqrt{N}$ for the regular quantum quench, $t_{\text{Ehr}} \propto \log N$ for the quench at DPT and for the periodic kicking, while $t_{\text{rec}} \propto N$ for the quantum quench dynamics and $t_{\text{rec}} \propto \exp(\exp(N))$ for the chaotic period kicking.

$\alpha = 0$		Quantum quench	Quench at DPT	Periodic kicking
Scrambling	$t < t_{\text{Ehr}}$	t^2/N^3	$e^{\lambda t}$	$e^{\lambda t}$
	$t_{\text{Ehr}} < t < t^*$	t^4/N^4	t/N	const.
Entanglement	$t < t_{\text{Ehr}}$	growth	peak	growth
	$t_{\text{Ehr}} < t < t^*$	const.	const.	const.

This shows that the state’s entanglement growth and operator’s scrambling are two distinct, apparently disconnected phenomena. Interestingly, this becomes glaringly obvious in the regular regime rather than in the chaotic one, see Fig. 4.

III. THE MODEL AND OUT-OF-EQUILIBRIUM PROTOCOLS

We consider an Ising chain in transverse field with long-range interactions,

$$\hat{H} = -\frac{1}{2} \sum_{i \neq j}^N J_{ij} \hat{\sigma}_i^z \hat{\sigma}_j^z - h \sum_i^N \hat{\sigma}_i^x, \quad (1)$$

where $\hat{\sigma}_i^x$, $\hat{\sigma}_i^z$ are spin operators and $J_{ij} = J|i - j|^{-\alpha}/N(\alpha)$ and $N(\alpha) = \sum_{r=1}^N 1/r^\alpha$ is the Kac normalization [47]. The (solvable) infinite range limit $\alpha = 0$ of Eq. (1) is known as the Lipkin-Meshov-Glick model (LMG) [48] and it has been intensively studied out-of-equilibrium [6,49–52]. In this case, the Hamiltonian conserves the total spin and we restrict our analysis to the sector of the ground state $S = N/2$. This has a semiclassical limit before t_{Ehr} , controlled by $\hbar_{\text{eff}} = \hbar/N$, where the system can be described classically in terms of only two degrees of freedom $\{Q, P\}$ and a classical Hamiltonian [6,49,50]. For finite N , ground states of the Hamiltonian Eq. (1) can be seen as coherent wave packets with width $\sigma \sim \sqrt{\hbar_{\text{eff}}}$ that evolve for short times classically [6]. The semiclassical dynamics is discussed in detail in the next section. As far as the dynamics of local observables is concerned, the Hamiltonian of Eq. (1) is found to behave as the infinite-range one for $\alpha < 1$, as a short-range one for $\alpha > 2$ [7,10].

Taking an initial separable state totally polarized along the z axis $|\psi_0\rangle = |\uparrow\uparrow\dots\uparrow\rangle$, we probe entanglement dynamics and scrambling with the two following protocols:

(a) *Quantum quench.* The state $|\psi_0\rangle$ is evolved with the Hamiltonian Eq. (1) with a transverse field h_f . For $\alpha \leq 1$, a special case, important also for the present analysis, is represented by $h_f = h_c = \frac{1}{2}$, where a DPT occurs [53], whose origin can be traced back to the corresponding classical dy-

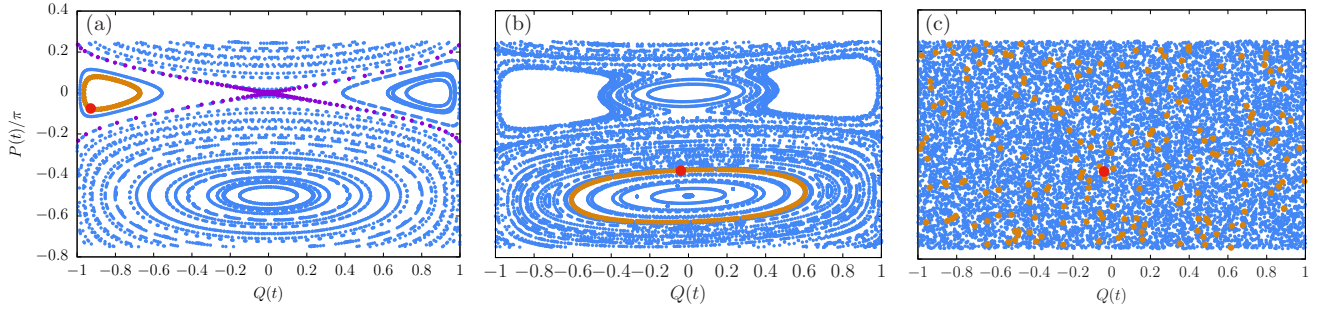


FIG. 1. Classical phase space (a) and Poincaré sections of the classical limit of the model (b), (c). (a) Phase space for the Hamiltonian of Eq. (4) for $h_f = \frac{1}{2}$. In purple, the separatrix between orbits with $\bar{Q} = 0$ and $\bar{Q} \neq 0$, which corresponds to the ground-state energy for $h_0 = 0$. (b) Regular Poincaré section for $K = 0.2$: we see that the dynamics remains always regular and each trajectory is a closed curve. (c) Chaotic Poincaré section for $K = 20$: the system clearly becomes chaotic and the trajectories tend to cover all the phase space ($h_f = 2$, $\tau = 1$). The red dot in the plots represents the initial condition in the classical limit, while the orange points represent its stroboscopic evolution.

namics. Away from the dynamical critical point, the Ehrenfest time reads $t_{\text{Ehr}}^r \propto \sqrt{N}$ while at the dynamical critical point $t_{\text{Ehr}}^c \propto \log N$. It was shown in Ref. [39] that DPT can be detected with the average value of out-of-time correlators.

(b) *Periodic kicking.* To address chaotic dynamics in a long-range spin system, we will also consider the case in which periodic kicks are added to the evolution governed by Eq. (1), with $\alpha = 0$. This model, known also as the “kicked top” for $h = 0$, is a paradigmatic example of the standard quantum chaos [54,55]. The time-evolution operator over one period reads

$$\hat{U} = \hat{U}_k \exp[-i\hat{H}\tau] \text{ with } \hat{U}_k \equiv \exp\left[-i\frac{2K}{N}\hat{S}_z^2\right]. \quad (2)$$

Depending on the value of the kicking strength K , this model is known to exhibit a transition between a regular regime and a chaotic one [54,55]. When $K \gg 1 \forall h_f$, orbits deviate exponentially in time and $t_{\text{Ehr}}^c \propto \log N$.

A. Semiclassical phase-space

Let us recall the main features of the semiclassical dynamics. Since the Hamiltonian of Eq. (1) commutes with the total spin $\hat{S} = \sum_i \hat{S}_i$, we restrict ourselves to the spin subsector of the ground state $S = N/2$, where the dimensionality of the Hilbert space is $N + 1$. Defining $\hat{\mathbf{m}} \equiv \hat{S}/S$, we can re-express the LMG Hamiltonian in terms of its components:

$$\hat{H}_{\text{LMG}} = -N\left(\frac{J}{2}\hat{m}^z{}^2 - h\hat{m}^x\right). \quad (3)$$

This allows us to consider an effective $\hbar_{\text{eff}} = \frac{\hbar}{N}$ that identifies the semiclassical limit with the large- N mean field one. In what follows we set $\hbar = 1$. In this limit, the system is effectively described by the classical Hamiltonian

$$\mathcal{H}_0(Q, P) \equiv -\frac{J}{2}Q^2 - h\sqrt{1-Q^2}\cos(2P), \quad (4)$$

where the two conjugate variables Q, P are given in terms of the expectation values of $\hat{\mathbf{m}}$ on a wave packet as $m^z = Q$, $m^x = \sqrt{1-Q^2}\cos(2P)$ and $m^y = \sqrt{1-Q^2}\sin(2P)$ and obey the classical Hamilton equations [6,49,50].

In the sudden quench case, the ground state at h_0 is evolved with the Hamiltonian with transverse field h_f . The DPT between a finite and zero-order parameter occurs at $h_f = h_c =$

$(h_0 + 1)/2$. One can define a dynamical order parameter as the average magnetization in time: $\bar{Q} = \lim_{T \rightarrow \infty} \int_0^T Q(s)ds$, which is different from zero in the symmetry broken phase. Indeed, at h_c the phase point associated with the initial ground-state energy (which is conserved) lays right on the separatrix of the final Hamiltonian: for $h_f > h_c$, it orbits around the maximum with a $\bar{Q} = 0$, while for $h_f < h_c$ it orbits around one of the two ferromagnetic minima and $\bar{Q} \neq 0$, see Fig. 1.

When the kicking is added, the total classical Hamiltonian reads

$$\mathcal{H}(Q, P, t) = \mathcal{H}_0(Q, P) + \mathcal{H}_{\text{kick}}(Q, P) \sum_n \delta(t - n\tau), \quad (5)$$

where $\mathcal{H}_{\text{kick}}(Q, P) = -\frac{K}{2}Q^2$: the classical kicking acts every period τ like a rotation around the z axis with an angle proportional to m_z . In the numerical calculations, we re-express the Hamilton equations of motion as equations of motion for the spin-components \mathbf{m} :

$$\begin{aligned} \dot{m}^x(t) &= 2Jm^y(t)m^z(t), \\ \dot{m}^y(t) &= 2hm^z(t) - 2Jm^x(t)m^z(t), \\ \dot{m}^z(t) &= -2hm^y(t). \end{aligned} \quad (6)$$

Note that these equations can be obtained also from the expectation value of the Heisenberg equation of motion, setting to zero the second-order cumulant. This is justified by the fact that the magnetization components commute in the classical limit: $[\hat{m}^\alpha, \hat{m}^\beta] = \frac{i}{N/2}\epsilon_{\alpha\beta\gamma}\hat{m}^\gamma$. In the limit of large but finite N , one can consider the semiclassical WKB approximation [6] and explore wave-packet dynamics. In this framework, ground states of \mathcal{H}_0 can be seen as coherent wave packets with width $\sigma = \sqrt{\hbar_{\text{eff}}} = 1/\sqrt{N}$. This semiclassical picture holds until the states behave like well-defined wave packets. It is then natural to define the time for which semiclassics breaks down—the *Ehrenfest time*—as the time for which the initially coherent wave packet is spread and delocalized. It is well known that this depends on the nature of the classical dynamics [56]:

$$t_{\text{Ehr}} \sim \begin{cases} \frac{1}{\sqrt{\hbar_{\text{eff}}}} = \sqrt{N} & \text{regular} \\ \frac{1}{2\lambda} \ln \frac{1}{\hbar_{\text{eff}}} = \frac{1}{2\lambda} \ln N & \text{chaotic/unstable} \end{cases}, \quad (7)$$

where $\lambda > 0$ is the Largest Lyapunov exponent of the classical dynamics in the chaotic case.

B. Characterization of chaos

In the quantum realm, an important signature of chaos is provided by the spectral properties of the evolution operator, in our case by the properties of the Floquet spectrum. The distribution of the Floquet level spacings $\delta_\alpha \equiv \mu_{\alpha+1} - \mu_\alpha$ (the μ_α are in increasing order), normalized by the average density of states, gives information on the integrability and ergodicity properties of the system [55,57–59]: if the distribution is Poisson, then the system is integrable; if it is Wigner-Dyson, then the system is ergodic. To probe the integrability/ergodicity properties through the level-spacing distribution, we consider the so-called level-spacing ratio:

$$0 \leq r_\alpha \equiv \frac{\min\{\delta_\alpha, \delta_{\alpha+1}\}}{\max\{\delta_\alpha, \delta_{\alpha+1}\}} \leq 1. \quad (8)$$

The different level spacing distributions are characterized by a different value of the average $r \equiv \langle r_\alpha \rangle$ over the distribution. From the results of Ref. [60], we expect $r = 0.386$ if the system behaves integrably and the distribution is Poisson; on the other side, if the distribution is Wigner-Dyson and the system behaves ergodically, then $r = 0.5295$. In our case, the Floquet levels fall in two symmetry classes, according to the corresponding Floquet state being an eigenstate of eigenvalue $+1$ or 1 of the operator $e^{i\pi\hat{S}_x}$, under which the Hamiltonian is symmetric [54]. Therefore we need to evaluate the level spacing distribution and the corresponding r only over Floquet states in one of the symmetry sectors of the Hamiltonian. The level spacing ratio for this model is reported in Fig. 2 as a function of the kicking strength K : it shows a transition from a regular to a chaotic regime.

The relationship between classical chaos and the properties of the many-body quantum dynamics has been widely studied in the past, giving rise to a plethora of signatures of chaos in the quantum domain [55,57]. Classically, a system is ergodic if all the trajectories uniformly explore the accessible part of the phase space. In the case of few degrees of freedom,

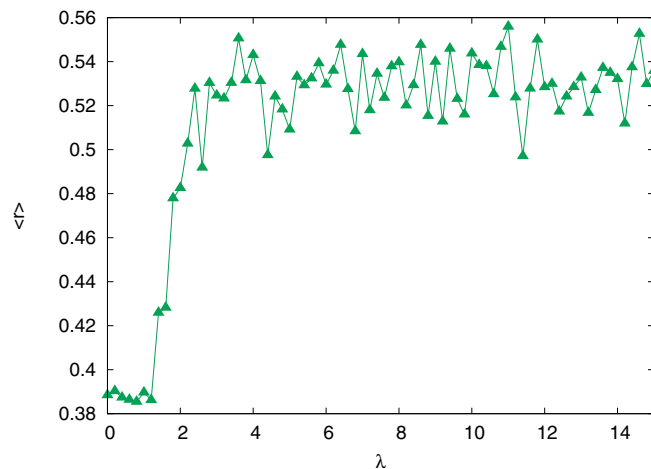


FIG. 2. Regular-chaotic transition witnessed by the average level spacing ratio. ($N = 1000$, $\tau = 1$, $h = 2$). Throughout the paper, we always chose $K = 20$, which clearly displays chaotic dynamics.

a qualitative measure of this phenomenon is the Poincaré section: some initial values are evolved under the stroboscopic dynamics reporting on a P, Q plot the sequence of their positions. If the initial condition lies in a regular region of the phase space, our points will be over a one-dimensional manifold. If instead, the initial condition is in a chaotic region of the phase space, our points will fill a two-dimensional portion of phase space. The model under analysis satisfies these conditions in the semi-classical limit, see Fig. 1.

IV. CHARACTERIZATION OF ENTANGLEMENT AND SCRAMBLING

Let us now introduce the quantities that we will use to characterize entanglement and scrambling. As far as the entanglement is concerned, we will focus on the multipartite case (bipartite entanglement was already studied in Refs. [61,62]). The characterization of multipartite entanglement is more delicate than that of bipartite entanglement since there exists a zoo of possible measures and witnesses. We will focus here on the QFI $F_Q(t)$ and on the TMI $I_3(t)$ [33], which accounts for the information delocalization. We instead study scrambling via the square commutator $c(t)$.

The QFI is a witness of multipartite entanglement which has been shown to obey scaling at the equilibrium transition point [63] and is connected to the diagonal ensemble in the nonequilibrium case [64]. The QFI gives a bound on the size of the biggest entangled block. For example, given a system of N spins, if the QFI density $f_Q \equiv F_Q/N > k$, then there are at least $k + 1$ entangled spins [65,66]. For pure states, the QFI is given by an optimization over a generic linear combination of local spin operators of $F_Q(\hat{O}, t) = 4 \langle \Delta \hat{O}^2 \rangle_t$. Here, we consider collective spin operators $\hat{O} = \hat{S} = \frac{1}{2} \sum_i \hat{\sigma}_i$ and we maximize over the three directions.

The TMI is defined as $I_3(A : B : C) = I(A : B) + I(A : C) - I(A : BC)$, where A, B, C, D are four partitions and the quantity $I(A : B)$ is the mutual information between A, B . This takes into account information about A that is nonlocally stored in C and D such that local measurements of B and C alone are not able to reconstruct A . Usually, $I_3 < 0$ is associated with the delocalization of quantum information in the context of unitary quantum channels [33]. In this case, more appropriately, we study the delocalization of the initial state information under the dynamics, which is a complementary measure of entanglement.

Finally, to characterize the dynamics of scrambling, we will focus on the *square commutator* $c(t) = -\langle [\hat{B}(t), \hat{A}]^2 \rangle$. This object measures the noncommutativity induced by the dynamics between two initially commuting operators, \hat{A} and \hat{B} . It was introduced by Larkin and Ovchinnikov in Ref. [20], to describe semiclassically the exponential sensitivity to initial conditions and the associated Lyapunov exponent. By taking collective spin operators [29] $\hat{A} = \hat{B} = \hat{m}_z = \hat{S}_z/S$, the square commutator has a natural classical limit for $\hbar_{\text{eff}} \rightarrow 0$ [67]

$$c(t) = -\langle [\hat{m}^z(t), \hat{m}^z]^2 \rangle \rightarrow \hbar_{\text{eff}}^2 \overline{\{Q(t), Q(0)\}^2}, \quad (9)$$

where $Q(t) = \langle \hat{m}_z(t) \rangle$ on a coherent wave packet, $\{\cdot\}$ are the Poisson brackets of the corresponding classical trajectory,

and the average $\overline{(\cdot)}$ is performed over an initial phase-space distribution.

V. METHODS

The results presented in this paper were obtained with a series of numerical techniques and two semianalytical approximations.

The numerical methods are a combination of exact diagonalization (ED) and well-established semiclassical approximations which are based on Wigner phase-space representations: the truncated Wigner approximation (TWA) [68] on the continuum phase-space and the discrete truncated Wigner approximation (DTWA) [45,69] of the finite dimensional phase space. To this end, we generalized the corresponding expression for the square commutator to the discrete phase-space representation, see Eq. (20) and the Supplementary Material for the details used in our calculations. All these approaches neglect terms of the order of $\mathcal{O}(1/N)$ and give the same results up to the Ehrenfest time. DTWA, in particular, is also able to reproduce entanglement long-time dynamics. Furthermore, we also adopted the matrix product state time-dependent variational principle (MPS-TDVP) [42,43], for the dynamics of long-range Hamiltonians with $\alpha \neq 0$.

We combine these approaches with two semianalytical methods to predict the behavior of $c(t)$ up to t_{Ehr} . The first method is a *equation of motion closure at fifth order*: it consists of deriving a hierarchy of differential equations for the square commutator and in closing it by setting the fifth-order cumulant to zero. This allows us to decouple the higher order commutator and to close the system of equations. By setting the appropriate initial conditions, one can integrate numerically the equations and get the approximated $c(t)$. The second method is a *time-dependent Holstein Primakoff* and it consists of including quantum fluctuations on top of the classical result and to keep it only at the Gaussian level. These approaches turn out to be equivalent and to correctly reproduce $c(t)$ before t_{Ehr} as in Fig. 3. The following two paragraphs are devoted to a description of these approximations.

A. Equation of motion closure at fifth order

The cumulant closure at order n is a general method that consists of closing a set of differential equations by setting to zero all cumulants of the order $\geq n$. A very easy example is the cumulant closure at second order, which allows computing the classical equation of motion for the magnetization of Eq. (6). We are interested in the dynamics of the square commutator and we wish to find a set of differential equations that gives its evolution.

One first defines a symmetric $(n + m + 2)$ -string commutator:

$$\begin{aligned} c_{\alpha_1, \dots, \alpha_n, \beta_1, \dots, \beta_m}(t) = & -\frac{1}{2} \langle [\hat{m}^{\alpha_1}(t) \hat{m}^{\alpha_2}(t) \dots \hat{m}^{\alpha_n}(t), \hat{m}^z] \\ & \times [\hat{m}^{\beta_1}(t) \hat{m}^{\beta_2}(t) \dots \hat{m}^{\beta_m}(t), \hat{m}^z] \rangle \\ & -\frac{1}{2} \langle [\hat{m}^{\beta_1}(t) \hat{m}^{\beta_2}(t) \dots \hat{m}^{\beta_m}(t), \hat{m}^z] \\ & \times [\hat{m}^{\alpha_1}(t) \hat{m}^{\alpha_2}(t) \dots \hat{m}^{\alpha_n}(t), \hat{m}^z] \rangle, \end{aligned} \quad (10)$$

where there are $n + m$ time-dependent operators and two time-independent ones. Within this notation, the square com-

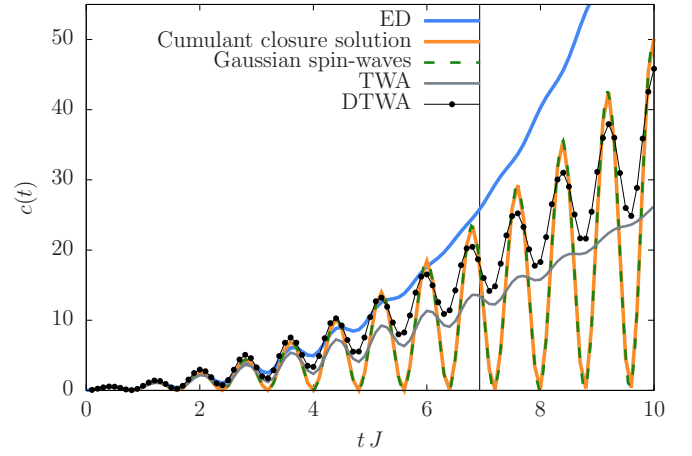


FIG. 3. Comparison between the different semiclassical approximations of the square commutator. Quantum quench dynamics with $h_f = 2$ and $N = 50$. All the approximated methods are found to reproduce the dynamics of $c(t)$ up to times t_{Ehr}^r , indicated with a thin line in the plot.

mutator of Eq. (1) reads $c(t) = c_{z,z}(t)$. The dynamics will generate an infinite number of coupled equations of motion. We close this hierarchy of differential equations by setting the fifth-order cumulant to zero: $\langle ABCDE \rangle_c = 0$. If one assumes that the magnetization is classical (second-order cumulant set to zero), the $(3 + 2)$ -string commutator decouples in

$$c_{\alpha, \beta \gamma}(t) + c_{\alpha, \gamma \beta}(t) = 2[m^\beta(t) c_{\alpha, \gamma}(t) + m^\gamma(t) c_{\alpha, \beta}(t)], \quad (11)$$

for $\alpha, \beta, \gamma \in \{x, y, z\}$. This allows us to close the hierarchy of differential equations, which are coupled to the classical magnetization dynamics of Eq. (6) as

$$\begin{aligned} \dot{c}_{z,z} &= -4h c_{z,y}, \\ \dot{c}_{z,y} &= -2h c_{y,y} + 2h c_{z,z} - 2J[c_{z,z} m^z + c_{z,x} m^x], \\ \dot{c}_{y,y} &= 4h c_{y,z} - 4J[c_{x,y} m^z + c_{x,y} m^z], \\ \dot{c}_{x,y} &= 2h c_{x,z} - 2J[c_{x,x} m^z + c_{x,z} m^x] \\ & \quad + 2J[c_{y,y} m^z + c_{y,z} m^y], \\ \dot{c}_{x,z} &= -2h c_{x,y} + 2J[c_{z,z} m^y + c_{z,y} m^z], \\ \dot{c}_{x,x} &= 2J[c_{x,z} m^y + c_{x,y} m^z]. \end{aligned} \quad (12)$$

These equations are integrated numerically via a fourth-order Runge-Kutta method. The information about the initial state and the dimension of the system is encoded in the initial conditions. The $c_{z,z}(t)$ that we obtain with this cumulant closure turns out to reproduce the limit $N \rightarrow \infty$ of all these semiclassical approximations. It well reproduces the exact $c(t)$, up to a time t_{Ehr}^r (see Fig. 3).

B. Time-dependent Holstein Primakoff

In a spin-wave expansion, quantum fluctuations are treated as small fluctuations on top of the classical solution [70]. One first produces a time-dependent rotation of the reference frame $\mathcal{R} = (\hat{X}(t), \hat{Y}(t), \hat{Z}(t))$, in such a way that the $\hat{Z}(t)$ axis follows the motion of the classical collective spin $\langle \hat{\mathbf{S}}(t) \rangle$.

Then a Holstein-Primakoff transformation is performed and the quantum fluctuations are kept at the Gaussian order. In this rotating frame, the collective spin operators are the zero-mode components in the Fourier transform: $\tilde{\sigma}_a^0$, with $a \in \mathcal{R}$. Our approximation consists of taking the operator on the Z axis not varying in time: $\tilde{\sigma}_Z^0(0) \sim \tilde{\sigma}_Z^0(t) + \mathcal{O}((N/2)^{-1})$. This allows us to compute commutators in the rotating frame, hence to get an approximated solution for $c(t)$.

The main steps to solve the dynamics are the following [70]:

(1) perform a time dependent unitary rotation with $V(\theta(t), \phi(t)) = e^{-i\frac{\phi(t)}{2}\sum_i \hat{\sigma}_i^z} e^{-i\frac{\theta(t)}{2}\sum_i \hat{\sigma}_i^y}$; the angles are chosen such that $\langle \hat{S}_X \rangle = \langle \hat{S}_Y \rangle = 0$. In the new frame the operators evolve with $\tilde{H} = V H V^\dagger + iV\dot{V}^\dagger$;

(2) perform an Holstein-Primakoff transformation on the operators in \mathcal{R} in terms of the conjugate variables $(\tilde{q}_0, \tilde{p}_0)$;

(3) keep only Gaussian terms, which is equivalent to neglect all $\mathcal{O}((N/2)^{-3/2})$ terms in the equations.

With such a choice, one remains with the following Hamiltonian:

$$\frac{\tilde{H}}{N} = h_{\text{class}}(t) + \frac{1}{\sqrt{Ns}} h_{\text{lin}}(t) + \frac{1}{Ns} h_{\text{quad}}(t) + \mathcal{O}((Ns)^{-3/2}), \quad (13)$$

where $h_{\text{class}}(t) = h \cos \theta - s \cos \theta \dot{\phi} - \frac{J}{2} \sin^2 \theta \cos^2 \phi$ is the classical Hamiltonian, $h_{\text{lin}}(t)$ contains linear terms in the quantum fluctuations (automatically zero on the classical solution) and $h_{\text{quad}}(t) = \frac{J}{2} \sin^2 \theta \cos^2 \phi \tilde{q}0^2 - \frac{J}{2} (\cos^2 \phi - \sin^2 \phi) \tilde{p}0^2 + J \cos \theta \sin \phi \cos \phi \frac{\tilde{p}0\tilde{q}0 + \tilde{q}0\tilde{p}0}{2} + J \cos^2 \phi \epsilon$ contains the quadratic terms in the quantum fluctuations, being ϵ the spin-wave populations defined in [70]. Then, by setting $\langle \hat{S}_X \rangle = \langle \hat{S}_Y \rangle = 0$, one gets the *equation of motion for the rotating frame*, see Ref. [71]:

$$\dot{\theta} = 2J \sin \theta \cos \phi \sin \phi, \quad \dot{\phi} = -2h + 2J \cos \theta \cos^2 \phi. \quad (14)$$

In the same way, one can obtain the Heisenberg equations of motion for \tilde{q}_0, \tilde{p}_0 . Further, defining the zero-mode fluctuations as

$$\Delta_0^{qq}(t) \equiv \langle \tilde{q}_0(t) \tilde{q}_0(t) \rangle, \quad (15a)$$

$$\Delta_0^{pp}(t) \equiv \langle \tilde{p}_0(t) \tilde{p}_0(t) \rangle, \quad (15b)$$

$$\Delta_0^{qp}(t) \equiv \frac{1}{2} \langle \tilde{q}_0(t) \tilde{p}_0(t) + \tilde{p}_0(t) \tilde{q}_0(t) \rangle, \quad (15c)$$

and combining them with the equations for \tilde{q}_0, \tilde{p}_0 , one gets the *equations of motion for the zero-mode fluctuations*

$$\begin{aligned} \dot{\Delta}_0^{qq} &= 4J \cos \theta \sin \phi \cos \phi \Delta_0^{qq} + 4J (\cos^2 \phi - \sin^2 \phi) \Delta_0^{pq}, \\ \dot{\Delta}_0^{pp} &= -4J \cos \theta \sin \phi \cos \phi \Delta_0^{pp} - 4J \cos^2 \phi \sin^2 \theta \Delta_0^{pq}, \\ \dot{\Delta}_0^{pq} &= -2J \cos^2 \phi \sin^2 \theta \Delta_0^{qq} + 2J (\cos^2 \phi - \sin^2 \phi) \Delta_0^{pp}. \end{aligned} \quad (16)$$

They are a set of linear time-dependent differential equations, which can be solved numerically with the appropriate initial conditions. They are exactly the quantities that appear in the computation of the square commutator. To compute it, perform first a rotation $\tilde{\sigma}_0^a(t)$ to $\tilde{\sigma}_0^a(t)$ with $V(\theta(t), \phi(t))$, then

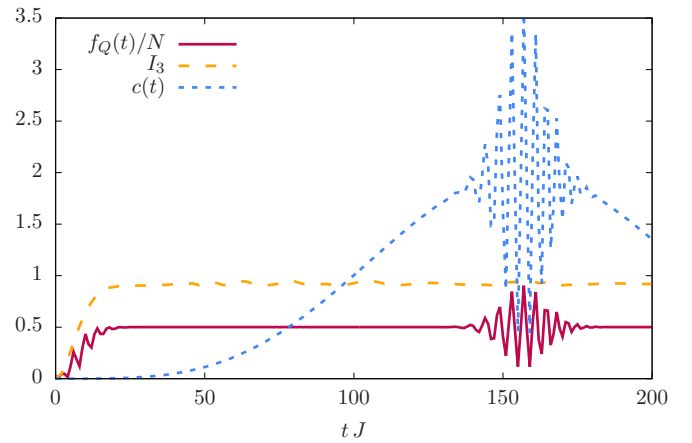


FIG. 4. Quantum information dynamics for the regular dynamics. The entanglement quantities, QFI and TMI (red and yellow), saturate at t_{Ehr} , while the square commutator of the longitudinal magnetization operator (blue) goes beyond semiclassics and keeps growing up to t^* . Exact diagonalization results for $N = 100$, $h_f = 2$, TMI with $n_A = 1$, $n_B = 10$ and $n_C = 20$.

compute commutators like $[\tilde{\sigma}_0^a(t), \tilde{\sigma}_0^Z]$, noticing that $\tilde{\sigma}_0^Z(0) = \tilde{\sigma}_0^Z(t) + \mathcal{O}((Ns)^{-1})$, hence at this order they are equal-time commutators and give rise to the zero-mode fluctuations of Eq. (15). For example, our square commutator of Eq. (3) reads as

$$c(t) = \sin^2 \phi \Delta_0^{pp} + \cos^2 \theta \cos^2 \phi \Delta_0^{qq} - 2 \cos \theta \sin \phi \cos \phi \Delta_0^{pq}, \quad (17)$$

which can be obtained numerically from the integration of Eq. (16) and gives exactly the same result of the previous approximation, see Fig. 3. This is correct until the spin-wave density remains small, which, for finite N , occurs before t_{Ehr} .

Notice that this method could be, in principle, extended to long-range systems with $\alpha \neq 0$ and other variations of fully connected models [70]. In addition, one could, in principle, go beyond the Gaussian approximation by keeping the interaction between spin waves.

VI. RESULTS

As we hinted at the beginning of the paper, entanglement and scrambling are two different phenomena, characterized by different timescales, see Fig. 4. Let us now finally describe in detail the results obtained for the dynamics of entanglement and scrambling using the methods described before.

A. Entanglement dynamics

In the infinite range model, entanglement dynamics and information delocalization reflect the semiclassical nature of the system under analysis. We start discussing the dynamics governed by Eq. (1) after a quantum quench and describe afterward the case of the periodic kicking protocol.

Let us focus first on the LGM model at $\alpha = 0$. Both $f_Q(t)$ and $I_3(t)$ have the same dynamics; growth followed by saturation at t_{Ehr} , as dictated by the semiclassical dynamics of the model, see Fig. 5 (top and middle panels). The stationary

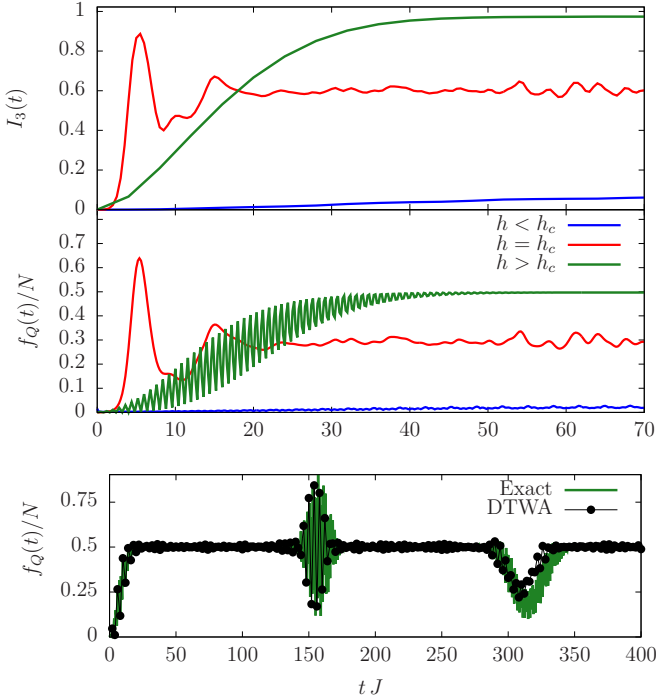


FIG. 5. QFI and TMI (top and middle) during the evolution after a quantum quench, performed below, at, and above the DPT. Entanglement grows in time up to t_{Ehr}^r for quenches above and below the dynamical phase transition (green and blue) and at t_{Ehr}^c at the critical point. Long-time dynamics (bottom) of the QFI, compared with the semiclassical approximation. The DTWA is able to reproduce the dynamics up to t_{rec}^r and beyond. Top and middle: $N = 450$, $h_f = 0.2$, $h_f = 0.5$ and $h_f = 2$; for the I_3 : $n_A = 1$, $n_B = 50$, $n_C = 200$. Bottom: $N = 100$ and $h_f = 2$, DTWA obtained with $5 \cdot 10^3$ samplings.

state displays global entanglement of genuine multipartite nature $f_Q = \phi_Q N$, where $\phi_Q \leq 1/2$ is a function of the transverse field. The value of the phase ϕ_Q along the z direction can be computed analytically in terms of elliptic integrals. Following Ref. [71], with a combination of the classical equation of motion and energy conservation, defining $k = J/2h \geq 1$, one gets

$$\phi_Q^z = \frac{1}{k^2} \left[(k^2 - 1) + \frac{E(\theta_k, k)}{F(\theta_k, k)} - \left(\frac{\pi}{2F(\theta_k, k)} \right)^2 \right], \quad (18)$$

where $F(\phi, k)$, $E(\phi, k)$ are the elliptic integrals of first and second kind of amplitude ϕ , modulus k and $\theta_k = \arcsin(1/k)$ is the inversion point of the classical trajectory $Q(t)$. The maximum asymptotic entanglement witnessed by the QFI is $\overline{f_Q} = \frac{N}{2}$, which occurs when the system from a product state is quenched to the maximally paramagnetic phase and corresponds to the biggest fluctuations of the collective spin operators.

The TMI gives complementary information: being positive, $\overline{I_3} > 0$ shows that the information of the initial state is not delocalized across the system. Interestingly, by increasing α the TMI becomes negative $I_3 < 0$, see Fig. 6.

Let us spend a few words for the quench to the DPT, which occurs at $h_c = 1/2$, see Sec. III. In this case, the entanglement

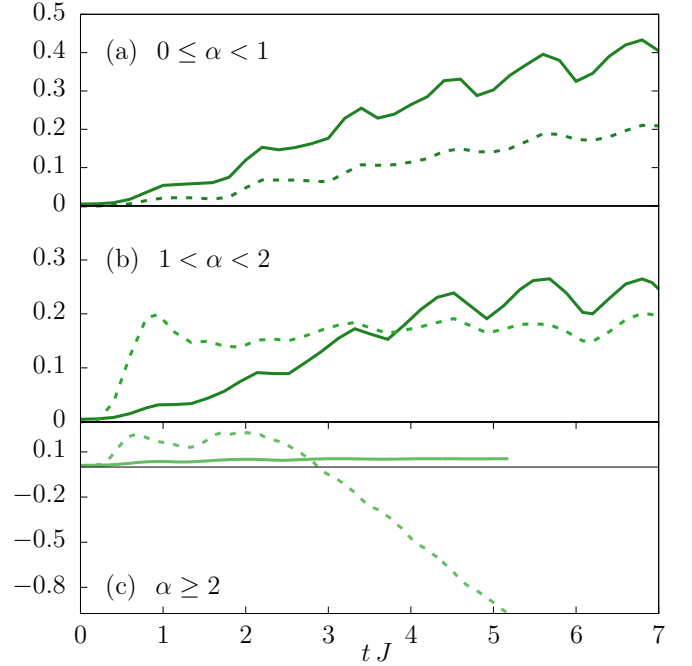


FIG. 6. We plot the minimal TMI (dotted lines) and the $f_Q(t)/N$ (full lines) as a function of time, varying the range of interaction α . We obtain the minimal TMI by calculating the tripartite mutual information for all possible partitions A,B,C,D of the system and then taking the minimum. For $0 \leq \alpha < 1$ (a), the dynamics is the same as the LMG model. For $1 \leq \alpha < 2$ (b), we observe linear growth of the QFI with time, whereas the minimum of the tripartite mutual information remains bounded with time. When $\alpha > 2$ (c), the QFI does not scale with the system size and remains bounded, whereas the minimum of the TMI decreases linearly with time and becomes negative for longer times. We present the detailed scaling with the system size in the Supplemental Material [76]. The parameters of the evolution are: $\alpha = 0.5$, $\alpha = 1.5$, $\alpha = 2.5$, $h_f = 0.75$. Data obtained with TDVP for system sizes $N = 200$ and bond dimension $D = 256$ (or $N = 100$, $D = 512$ for $\alpha = 2.5$).

dynamics is qualitatively different. QFI and TMI at short times peak at t_{Ehr}^c . After a transient, they reach their stationary value, which keeps oscillating without recurrences, see Fig. 5. This behavior is tightly linked to the existence of the DPT, that corresponds to a classical separatrix in phase space: the effective classical trajectory takes time of the order of $\log N$ to depart from its initial value. After that, the classical picture is lost and the state is spread over the basis giving a constant entanglement, see Fig. 5.

The entanglement dynamics is reproduced, up to very long times, by a semiclassical approach. We studied this regime using DTWA, spin-wave theory and cumulant closure methods, see Sec. V in the Appendix. All these approaches neglect terms of the order of $\mathcal{O}(1/N)$ and give the same results up to the Ehrenfest time. The accuracy of all the semiclassical analysis is justified by the entanglement structure itself. In fact, this is what lies at the heart of the classical ‘‘simulability’’ of quantum long-range interacting systems in the context of MPS-TDVP [42,43] and with semiclassical methods [44–46]. DTWA, in particular, is able to reproduce also the long-time dynamics even beyond the recurrence time $t_{\text{rec}}^r \propto N$ as shown

in Fig. 5 (bottom panel). This is due to the fact that this method averages over an extensive number of trajectories, hence mimicking the discreteness of the spectrum, responsible for the recurrences [45].

The same asymptotic structure and dynamics is found for all mean-field-like systems $0 \leq \alpha < 1$: the QFI grows linearly in time up to a value $\sim N$, and the TMI increases logarithmically in time up to a constant value. For $1 \leq \alpha < 2$, the QFI and the TMI grow linearly in time and the entanglement structure of the asymptotic state is the same as for $\alpha < 1$. Decreasing the range of interaction the situation changes drastically: for $\alpha \geq 2$, the state displays the typical dynamics and structure of short-range interacting systems $\overline{f_Q} \sim \text{const}$; interestingly, $\overline{I_3} < 0$ signaling that the information about the initial condition is spread throughout the degrees of freedom of the state (see Fig. 6). The results are obtained with TDVP, see the Ref. [76] for a discussion of the convergence of the method.

Finally, we conclude the analysis of the multipartite entanglement by considering the kicked case in the regime when the dynamics is chaotic. This system heats up to a state where all local observables on any Floquet state correspond to the infinite temperature values [54]. All quantities characterizing entanglement saturate to an asymptotic value at the Ehrenfest time t_{Ehr}^c , for every initial state and field h , see Fig. S4 of the Ref. [76]. The value of the QFI, being a sum of local observables, is compatible with the values of the infinite temperature state: $\overline{f_Q} = 1 + \frac{N}{3} + \mathcal{O}(1/N)$. On the other side, the entanglement entropy saturates to the value expected for a random state, which was derived by Page in Ref. [72] $S_{\text{Page}} = \log m - \frac{m}{2n} + \mathcal{O}(1/mn)$, with m, n the dimensions of the Hilbert space of the two subsystems, and $m \leq n$. In this case, for a partition of size L the dimensions are $m = L + 1$, $n = N - L + 1$ and $S_{\text{Page}} = \log(L + 1) + \mathcal{O}(1/N)$. This reflects in the TMI and we find

$$\overline{I_3} = \log(\tilde{n}) \quad \text{with} \\ \tilde{n} = \frac{(n_A + 1)(n_B + 1)(n_C + 1)(n_A + n_B + n_C + 1)}{(n_A + n_B + 1)(n_A + n_C + 1)(n_B + n_C + 1)}. \quad (19)$$

B. Scrambling

Scrambling, as measured by the square commutator, behaves in a way profoundly different from entanglement. It is characterized by an initial semiclassical regime and a second quantum nonperturbative growth. Interestingly, this phenomenon is very evident in the regular regime (Fig. 7), and it is much less clear in the chaotic one (Fig. 8) already discussed at the beginning of the paper.

In the case of the quench dynamics, for $h_f \gg h_c$ the square commutator is characterized by a first semiclassical quadratic growth $c(t) \propto t^2/N^3$ until t_{Ehr}^c . In this regime, semiclassical approximations describe very well the evolution of $c(t)$ and we choose to employ DTWA. To this end, we generalize the corresponding expression for the square commutator to the discrete phase space representation:

$$c(t) \sim \frac{\hbar^2}{N^4} \sum_{i,j,k,m} [\delta_{ij}^{xzy}(t) - \delta_{ij}^{yzx}(t)] [\delta_{km}^{xzy}(t) - \delta_{km}^{yzx}(t)], \quad (20)$$

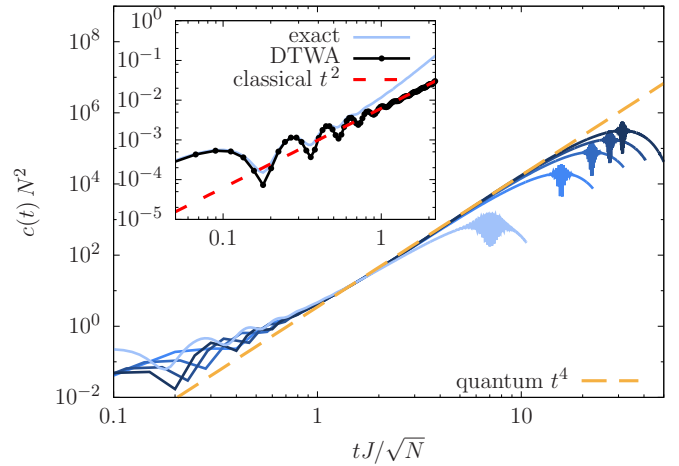


FIG. 7. The two-times regime of the square commutator in the LMG model after a quantum quench with $h_f = 2$. In the main plot, the quantum regime of $c(t)$ for different N : this regime starts at \sqrt{N} and then $c(t)$ grows polynomially as t^4 . ED results in blue for $N = 20, 100, 200, 300, 400$ (increasing color darkness), dashed yellow line for the polynomial fit. In the insert, we show the semiclassical regime, comparing the exact $c(t)$ with DTWA, which predicts the $\sim t^2$ power-law growth, dashed in the plot. Here $N = 20$ and DTWA obtained with $5 \cdot 10^3$ samplings.

where $\delta_{ij}^{\alpha\beta\gamma}(t) = \sigma_i^\alpha(0) \frac{\partial \sigma_j^\beta(t)}{\partial \sigma_i^\gamma(0)}$, with $\sigma_i^{x,y,z}$ the Weyl transform of the spin operators and the average $\overline{(\cdot)}$ is computed over the initial discrete Wigner distribution, see Ref. [76]. At t_{Ehr}^c the quantum regime starts, characterized by a polynomial growth $\sim (t/N)^4$ up to a maximum $c(t_{\text{Ehr}}^c) \sim 2$. At this time, the square commutator is independent of the system size. Even the

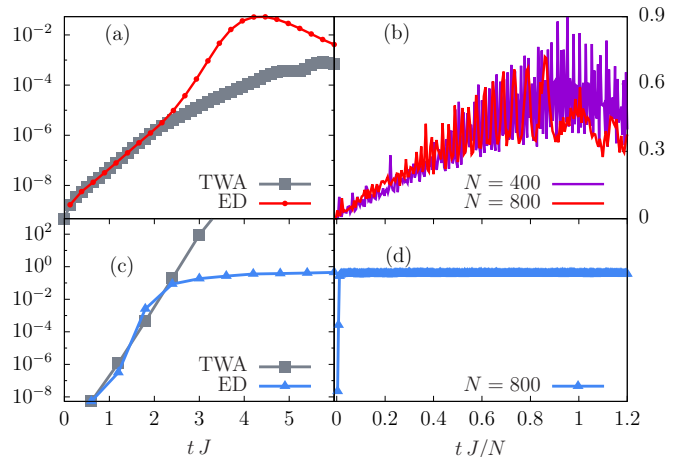


FIG. 8. Square commutator dynamics $c(t)$ for the LMG model after a quantum quench to the DPT point (a), (b) and for the kicked top with $K = 20$, $h_f = 2$, $\tau = 0.6$ (c), (d). At early times (a), (c), they are both characterized by an exponential growth up to t_{Ehr}^c , see the right side with the log scale on the y axis. This regime can be perfectly reproduced by the TWA (b), (d). At long times, the behavior is different depending on the quantum integrability properties. In (c), the time is rescaled by N to show that $c(t)$ grows up to a maximum at t_{Ehr}^c . In (d), in the kicked top, the $c(t)$ stays constant also at very long times. In (a) and (c), we used $N = 800$ and TWA obtained with 10^4 samplings.

DTWA, that perfectly reproduces multipartite entanglement dynamics up to t_{rec}^r (see Fig. 5), is not able to reproduce the long-time dynamics of the square commutator, see Fig. 7. Indeed, DTWA, despite keeping N discrete trajectories, represents all operators as factorized on each site at any time [45]. At times longer than t_{Ehr} , the operator expansion starts developing longer and longer strings and the square commutator resums all the correlations, until t_*^r , which corresponds to the time at which the string of length N occurs. Quenches to $h_f \ll h_c$ are characterized by the same timescales t_{Ehr}^r and t_*^r and the same semiclassical regime $\sim t^2/N^3$ up to t_{Ehr}^r . The result at long times is qualitatively different: the quantum regime is $\sim t^3/N^4$ and $c(t_*^r) \sim 10^{-3}/N$ goes to zero at all times in the thermodynamic limit. This is a direct consequence of the existence of the dynamical transition, which is detected by scrambling [39]. Due to the presence of a macroscopic magnetization, the support of the operators has a constrained dynamics and it will not acquire a string of length N .

A special case is represented by the quench at $h_f = h_c$; despite the integrability of the quantum system, we find that the square commutator grows exponentially in time up to t_{Ehr}^c as $c(t) = e^{2t}/N^3$. This is due to the existence of the unstable trajectory in the classical dynamics. The exponent is twice the eigenvalue of the instability matrix of the separatrix trajectory $\lambda_{h_c} = 2\sqrt{h_c(1-h_c)}$ for $h_c = 1/2$. This is valid in general for all the classical trajectories associated with DPT. To our knowledge, it is the only example of an early-time exponential growth in a many-body regular system.

After t_{Ehr}^c , $c(t)$ keeps growing linearly in time up to the t_*^c , then it goes back, see Fig. 8. Long-range interactions do not drastically change this finding. In the range $\alpha < 1$, the early-time dynamics is the same as that described before. The square commutator grows like a power law at small times, even for $\alpha > 2$.

We conclude by considering the kicking, which induces a chaotic dynamics. As expected, $c(t)$ is initially dominated by the classical exponential growth, then, as $t \sim t_{\text{Ehr}}^c$, quantum interference effects appear and the square commutator saturates to a constant value [67], see Fig. 8 (lower panels). In the quantum chaotic regime, the dynamics is reproduced by the semiclassical approximation, which predicts the initial time growth of the square commutator. After t_{Ehr}^c , the TWA loses any physical meaning. The quantum $c(t)$ remains constant and finite in the thermodynamic limit, meaning that the operator support is spread up to the longest string already from t_{Ehr}^c . Notice that in this case, the exponent is different from the actual classical Lyapunov exponent, defined as $\lambda_L \equiv \lim_{T \rightarrow \infty} \lim_{\delta Q_0 \rightarrow 0} \log(|\delta Q(T)|/\delta Q_0)/T$, that we compute following [73]. As pointed out by Ref. [30], this difference comes from a different ordering in evaluating the phase-space averages.

VII. CONCLUSIONS

In this work we perform an analysis of the spreading of multipartite entanglement in long-range spin systems in comparison to that of scrambling. We show that quantum correlations build up and spread in different ways. While entanglement and the delocalization of the state's information are state properties, scrambling instead describes the growth of quantum correlations in operator's space.

After a quantum quench in the transverse field of the infinite range Hamiltonian, entanglement is seen to saturate and become extensively multipartite $\sim \phi_Q N$ at t_{Ehr} . On the same timescale, the TMI I_3 saturates to a positive value $I_3 > 0$, showing that the information of the initial state is not delocalized across the system. In this case, entanglement dynamics is reproduced, up to very long times, by all the semiclassical approaches. On the other end, scrambling, as characterized by the square commutator of collective spin operators, increases semiclassically up to t_{Ehr} , continuing its growth even afterward up to the recurrence time. Particularly interesting is that, despite the dynamics being regular, the early-time exponential behavior emerges when the dynamics occurs at the critical point of the DPT, see Fig. 8. This point is associated with an unstable trajectory on the effective classical phase-space [6] and the exponent of the square commutator is twice the eigenvalue of the instability matrix of the separatrix trajectory. Nonetheless, being the quantum dynamics regular, after t_{Ehr} , the square commutator keeps growing linearly in time up to t^* , see Fig. 8. The other quenches, as in Fig. 4, are characterized by a first growth $\propto t^2/N^3$ up to t_{Ehr} , which is followed by a polynomial quantum regime $\sim (t/N)^4$ up to t^* .

In the presence of a periodic kicking for the chaotic evolution, entanglement saturates at $t_{\text{Ehr}} \sim \log N$ to values compatible with the infinite temperature state. As far as scrambling is concerned, we recover the exponential growth of the square commutators expected for chaotic systems up to t_{Ehr} , followed by the corresponding saturation induced by quantum interference effects, see Fig. 8.

We conclude the summary of our results by considering the case in which a quantum quench is performed with $\alpha \neq 0$. In this case, we employ TDVP and semiclassical analysis. Entanglement has the same asymptotic structure and dynamics within the interaction range $0 \leq \alpha < 1$: the QFI grows linearly in time up to a value $\sim N$, and the TMI increases logarithmically in time up to a constant value. For $1 \leq \alpha < 2$, the QFI and the TMI grow linearly in time and the entanglement structure of the asymptotic state is the same as for $\alpha < 1$. Decreasing the range of interaction the situation changes: for $\alpha \geq 2$ the state displays the typical dynamics and structure of short-range interacting systems $\sim \text{const}$; interestingly, $I_3 < 0$, signaling that the information about the initial condition is spread throughout the degrees of freedom of the state (see Fig. 6). Coming to scrambling, we find that before t_{Ehr} for $\alpha < 1$, the square commutator grows as $\propto t^2$.

Despite entanglement can be efficiently reproduced up to very long times by our numerical tools, they all fail in predicting scrambling after t_{Ehr} . In our understanding, this follows from the fact that all methods approximate the support of the operator to remain factorized on the initial basis. Such approximations do not allow us to reproduce the nonlocal behavior of scrambling at long times. We would like to stress that the quantum regime of scrambling, which arises after t_{Ehr} is not peculiar only of our models or of regular dynamics. In fact, a power law in the quantum regime has also been found in chaotic systems [74,75]. The long-time behavior of the square commutator shows the presence of purely quantum correlations that build up in the operator space. In this respect, it would be interesting to explore new quantum information protocols that encode information in the operator itself.

ACKNOWLEDGMENTS

We acknowledge useful discussions with J. Goold, A. Lerose, and A. Polkovnikov. We acknowledge support from

EU through project QUIC under Grant Agreement No. 641122, the National Research Foundation of Singapore (CRP - QSYNC). B. Z. is supported by the European Research Council (ERC), Advanced Grant No. 694544 OMNES.

-
- [1] A. Campa, T. Dauxois, D. Fanelli, and S. Ruffo, *Physics of Long-Range Interacting Systems* (Oxford University Press, Oxford, 2014).
- [2] M. Albiez, R. Gati, J. Fölling, S. Hunsmann, M. Cristiani, and M. K. Oberthaler, *Phys. Rev. Lett.* **95**, 010402 (2005).
- [3] R. Blatt and C. Roos, *Nat. Phys.* **8**, 277 (2012).
- [4] P. Jurcevic, H. Shen, P. Hauke, C. Maier, T. Brydges, C. Hempel, B. P. Lanyon, M. Heyl, R. Blatt, and C. F. Roos, *Phys. Rev. Lett.* **119**, 080501 (2017).
- [5] B. Neyenhuis, J. Smith, A. C. Lee, J. Zhang, P. Richerme, P. W. Hess, Z.-X. Gong, A. V. Gorshkov, and C. Monroe, *Sci. Adv.* **3**, e1700672 (2017).
- [6] B. Sciolla and G. Biroli, *J. Stat. Mech.* (2011) P11003.
- [7] B. Žunkovič, M. Heyl, M. Knap, and A. Silva, *Phys. Rev. Lett.* **120**, 130601 (2018).
- [8] E. A. Yuzbashyan, O. Tsyplatyev, and B. L. Altshuler, *Phys. Rev. Lett.* **96**, 097005 (2006).
- [9] P. Hauke and L. Tagliacozzo, *Phys. Rev. Lett.* **111**, 207202 (2013)
- [10] L. Cevelani, G. Carleo, and L. Sanchez-Palencia, *New J. Phys.* **18**, 093002 (2016).
- [11] Z. X. Gong, M. Foss-Feig, S. Michalakis, and A. V. Gorshkov, *Phys. Rev. Lett.* **113**, 030602 (2014).
- [12] M. Foss-Feig, Z. X. Gong, C. W. Clark, and A. V. Gorshkov, *Phys. Rev. Lett.* **114**, 157201 (2015).
- [13] D. J. Luitz and Y. Bar Lev, [arXiv:1805.06895](https://arxiv.org/abs/1805.06895).
- [14] E. Lieb and D. Robinson, *Commun. Math. Phys.* **28**, 251 (1972).
- [15] M. B. Hastings and T. Koma, *Commun. Math. Phys.* **265**, 781 (2006).
- [16] L. Amico, R. Fazio, A. Osterloh, and V. Vedral, *Rev. Mod. Phys.* **80**, 517 (2008).
- [17] J. Eisert, M. Cramer, and M. B. Plenio, *Rev. Mod. Phys.* **82**, 277 (2010).
- [18] P. Calabrese, J. Cardy, and B. Doyon Eds, *J. Phys. A* **42**, 500301 (2009).
- [19] P. Calabrese and J. Cardy, *J. Stat. Mech.* (2005) P04010.
- [20] A. I. Larkin and Y. N. Ovchinnikov, *Sov. Phys. JETP* **28**, 1200 (1969).
- [21] A. Kitaev, talks at KITP, April 7, 2015 and May 27, 2015, Caltech & ICTP, Santa Barbara, CA, USA.
- [22] J. Maldacena and D. Stanford, *Phys. Rev. D* **94**, 106002 (2016).
- [23] J. Maldacena, S. H. Shenker, and D. Stanford, *J. High Energy Phys.* **08** (2016) 106.
- [24] M. Mezei and D. Stanford, *J. High Energy Phys.* **05** (2017) 065.
- [25] I. L. Aleiner, L. Faoro, and L. B. Ioffe, *Ann. Phys.* **375**, 378 (2016).
- [26] A. A. Patel and S. Sachdev, *Proc. Nat. Acad. Sci. U.S.A.* **114**, 1844 (2017).
- [27] B. Swingle and D. Chowdhury, *Phys. Rev. B* **95**, 060201 (2017).
- [28] X. Chen, T. Zhou, D. A. Huse, and E. Fradkin, *Ann. Phys.* **529**, 1600332 (2017).
- [29] I. Kukuljan, S. Grozdanov, and T. Prosen, *Phys. Rev. B* **96**, 060301 (2017).
- [30] E. B. Rozenbaum, S. Ganeshan, and V. Galitski, *Phys. Rev. Lett.* **118**, 086801 (2017).
- [31] T. Scaffidi and E. Altman, [arXiv:1711.04768](https://arxiv.org/abs/1711.04768).
- [32] J. Rammensee, J.-D. Urbina, and K. Richter, *Phys. Rev. Lett.* **121**, 124101 (2018).
- [33] P. Hosur, X. L. Qi, D. A. Roberts, and B. Yoshida, *J. High Energy Phys.* **02** (2016) 004.
- [34] D. Ding, P. Hayden, and M. Walter, *J. High Energy Phys.* **12** (2016) 145.
- [35] C. von Keyserlingk, T. Rakovszky, F. Pollmann, and S. Sondhi, *Phys. Rev. X* **8**, 021013 (2018).
- [36] Z. W. Liu, S. Lloyd, E. Y. Zhu, and H. Zhu, *Phys. Rev. Lett.* **120**, 130502 (2018).
- [37] M. Gärtner, P. Hauke, and A. M. Rey, *Phys. Rev. Lett.* **120**, 040402, (2018).
- [38] X. Chen, T. Zhou, and C. Xu, *J. Stat. Mech.* (2018) 073101.
- [39] M. Heyl, F. Pollmann, and B. Dóra, *Phys. Rev. Lett.* **121**, 016801 (2018).
- [40] B. Swingle, G. Bentsen, M. Schleier-Smith, and P. Hayden, *Phys. Rev. A* **94**, 040302 (2016).
- [41] M. Gärtner, J. G. Bohnet, A. Safavi-Naini, M. L. Wall, J. J. Bollinger, and A. M. Rey, *Nat. Phys.* **13**, 781 (2017).
- [42] J. Haegeman, C. Lubich, I. Oseledets, B. Vandereycken, and F. Verstraete, *Phys. Rev. B* **94**, 165116 (2016).
- [43] J. Haegeman, J. I. Cirac, T. J. Osborne, I. Pižorn, H. Verschelde and F. Verstraete, *Phys. Rev. Lett.* **107**, 070601 (2011).
- [44] A. Polkovnikov, *Ann. Phys.* **325**, 1790 (2010).
- [45] J. Schachenmayer, A. Pikovski, and A. M. Rey, *Phys. Rev. X* **5**, 011022 (2015).
- [46] J. Wurtz, A. Polkovnikov, and D. Sels, *Ann. Phys.* **395**, 341 (2018).
- [47] M. Kac, *J. Math. Phys.* **4**, 216 (1963).
- [48] H. J. Lipkin, N. Meshkov, and A. J. Glick, *Nucl. Phys.* **62**, 188 (1965).
- [49] V. Bapst and G. Semerjian, *J. Stat. Mech.* **2012** (2012) P06007.
- [50] A. Russomanno, R. Fazio, and G. E. Santoro, *Europhys. Lett.* **110**, 37005 (2015).
- [51] I. Homrighausen, N. O. Abeling, V. Zauner-Stauber, and J. C. Halimeh, *Phys. Rev. B* **96**, 104436 (2017).
- [52] J. Lang, B. Frank, and J. C. Halimeh, *Phys. Rev. B* **97**, 174401 (2018).
- [53] B. Žunkovič, A. Silva, and M. Fabrizio, *Philos. Trans. R. Soc. London A* **374**, 20150160 (2016).
- [54] F. Haake, M. Kuš, and R. Scharf, *Z. Phys. B* **65**, 381 (1987).
- [55] F. Haake, *Quantum Signatures of Chaos* (Springer Science and Business Media, Germany, 2013), Vol. 54.
- [56] R. Schubert, R. O. Vallejos, and F. Toscano, *J. Phys. A: Math. Theor.* **45**, 215307 (2012).
- [57] M. V. Berry, Les Houches Lecture Ser. **36**, 171 (1983).
- [58] O. Bohigas, M. J. Giannoni, and C. Schmit, *Phys. Rev. Lett.* **52**, 1 (1984).

- [59] P. Kos, M. Ljubotina, and T. Prosen, *Phys. Rev. X* **8**, 021062 (2018).
- [60] V. Oganesyan and D. A. Huse, *Phys. Rev. B* **75**, 155111 (2007).
- [61] J. Schachenmayer, B. P. Lanyon, C. F. Roos, and A. J. Daley, *Phys. Rev. X* **3**, 031015 (2013).
- [62] A. S. Buyskikh, M. Fagotti, J. Schachenmayer, F. Essler, and A. J. Daley, *Phys. Rev. A* **93**, 053620 (2016).
- [63] P. Hauke, M. Heyl, L. Tagliacozzo, and P. Zoller, *Nat. Phys.* **12**, 778 (2016).
- [64] S. Pappalardi, A. Russomanno, A. Silva, and R. Fazio, *J. Stat. Mech.* (2017) 053104.
- [65] P. Hyllus, W. Laskowski, R. Krischek, C. Schwemmer, W. Wieczorek, H. Weinfurter, L. Pezzé, and A. Smerzi, *Phys. Rev. A* **85**, 022321 (2012).
- [66] G. Tóth, *Phys. Rev. A* **85**, 022322 (2012).
- [67] J. S. Cotler, D. Dawei, and G. R. Penington, *Ann. Phys.* **396**, 318 (2018).
- [68] P. B. Blakie, A. S. Bradley, M. J. Davis, R. J. Ballagh, and C. W. Gardiner, *Adv. Phys.* **57**, 363 (2008).
- [69] W. K. Wootters, *Ann. Phys.* **176**, 1 (1987).
- [70] A. Lerose, J. Marino, B. Zunkovic, A. Gambassi, and A. Silva, *Phys. Rev. Lett.* **120**, 130603 (2018).
- [71] A. Das, K. Sengupta, D. Sen, and B. K. Chakrabarti, *Phys. Rev. B* **74**, 144423 (2006).
- [72] D. N. Page, *Phys. Rev. Lett.* **71**, 1291 (1993).
- [73] G. Benettin, L. Galgani, and J. M. Strelcyn, *Phys. Rev. A* **14**, 2338 (1976).
- [74] D. Bagrets, A. Altland, and A. Kamenev, *Nucl. Phys. B* **921**, 727 (2017).
- [75] D. Bagrets, A. Altland, and A. Kamenev, *Nucl. Phys. B* **911**, 191 (2016).
- [76] See Supplemental Material at <http://link.aps.org/supplemental/10.1103/PhysRevB.98.134303> for a brief recap on the semi-classical numerical approximate methods (TWA/DTWA) and more plots concerning entanglement dynamics.